OPTICS

On-demand photonic entanglement synthesizer

Shuntaro Takeda[1,2,3]*, Kan Takase[1], Akira Furusawa[1,2]*

Quantum information protocols require various types of entanglement, such as Einstein-Podolsky-Rosen, Greenberger-Horne-Zeilinger, and cluster states. In optics, on-demand preparation of these states has been realized by squeezed light sources, but such experiments require different optical circuits for different entangled states, thus lacking versatility. Here, we demonstrate an on-demand entanglement synthesizer that programmably generates all these entangled states from a single squeezed light source. This is achieved by a loop-based circuit that is dynamically controllable at nanosecond time scales and processes optical pulses in the time domain. We verify the generation of five different small-scale entangled states and a large-scale cluster state containing more than 1000 modes without changing the optical circuit. Moreover, this circuit enables storage and release of one part of the generated entangled state, thus working as a quantum memory. Our demonstration should open a way for a more general entanglement synthesizer and a scalable quantum processor.

INTRODUCTION

Entanglement is an essential resource for many quantum information protocols in both qubit and continuous variable (CV) regimes. However, different types of entanglement are required for different applications (Fig. 1A). The most commonly used maximally entangled state is a two-mode Einstein-Podolsky-Rosen (EPR) state (1), which is the building block for two-party quantum communication and quantum logic gates based on quantum teleportation (2, 3). Its generalized version is an n-mode Greenberger-Horne-Zeilinger (GHZ) state (4, 5), which is central to building a quantum network; this state, once shared between n parties, enables any two of the n parties to communicate with each other (5, 6). In terms of quantum computation, a special type of entanglement called cluster states has attracted much attention as a universal resource for one-way quantum computation (7–9).

Thus far, the convenient and well-established method for deterministically preparing photonic entangled states is to mix squeezed light via beam splitter networks and generate entanglement in the CV regime (10–12). By using squeezed light sources multiplexed in the time (12) or frequency (13) domain, generation of large-scale entangled states has also been demonstrated recently. In these experiments, however, optical setups are designed to produce specific entangled states. That is, the optical setup has to be modified to produce different entangled states, thus lacking versatility. A few experiments have reported programmable characterization of several types of entanglement in multimode quantum states by postprocessing on measurement results (14) or changing measurement basis (15, 16). However, directly synthesizing various entangled states in a programmable and deterministic way is still a challenging task.

Here, we propose an on-demand photonic entanglement synthesizer that can programmably produce an important set of entangled states, including an EPR state, an n-mode GHZ state, and an n-mode linear- or star-shaped cluster state for any $n \geq 2$ (Fig. 1A). This synthesizer is based on a dynamically controllable photonic circuit that processes optical pulses in the time domain. Using this circuit, we verify the programmable generation of various entangled states in Fig. 1B, including five different small-scale entangled states and a

large-scale cluster state containing more than 1000 modes. We also demonstrate that the implemented photonic circuit can store and release one part of the generated entangled state, thus working as a quantum memory. The implemented circuit is a core circuit to realize a more general entanglement synthesizer (8, 17) and a scalable quantum processor (18), thus offering a promising route to photonic quantum information processing with scalability and programmability.

RESULTS

Concept of entanglement synthesizer

The conceptual schematic of the entanglement synthesizer is shown in Fig. 2A. Squeezed optical pulses are sequentially produced from a single squeezer and injected into a loop circuit whose round-trip time τ is equivalent to the time interval between the pulses. This loop includes a beam splitter with variable transmissivity $T(t)$ and a phase shifter with variable phase shift $\theta(t)$, where t denotes time. After transmitting the loop, the pulses are sent to a homodyne detector with a tunable measurement basis $\hat{x}_{\phi(t)} = \hat{x} \cos \phi(t) + \hat{p} \sin \phi(t)$, where $\hat{x}$ and $\hat{p}$ are quadrature operators. By dynamically changing $T(t)$, $\theta(t)$, and $\phi(t)$ for each pulse as in Fig. 2B, this circuit can synthesize various entangled states from the squeezed pulses and analyze them. This functionality can be understood by considering an equivalent circuit in Fig. 2C. Here, the conversion from the squeezed pulses $1', 2', \dots$ to the output pulses $1, 2, \dots$ in Fig. 2C is completely equivalent to the corresponding conversion in Fig. 2A. It is known that all of the entangled states in Fig. 1A can be produced in the circuit of Fig. 2C as long as the beam splitter transmissivity ($T_1, T_2, \dots$) and phase shift ($\theta_1, \theta_2, \dots$) are arbitrarily tunable (see Materials and Methods) (5, 19). However, the circuit in Fig. 2C lacks scalability because one additional entangled mode requires one additional squeezer, beam splitter, and detector. In contrast, our loop-based synthesizer in Fig. 2A markedly decreases the complexity of the optical circuit and, even more, can produce any of these entangled states by appropriately programming the control sequence in Fig. 2B, without changing the optical circuit itself.
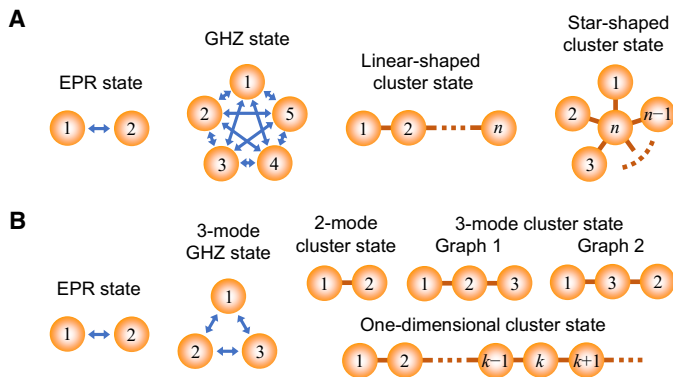
Synthesis of small-scale entangled states

We implement this synthesizer using a setup shown in Fig. 2D. Here, squeezed optical pulses arrive at a 19.8-m loop every $\tau = 66$ ns. We develop a technique to dynamically change the beam splitter transmissivity, phase shift, and measurement basis within 20 ns and time-synchronize the switching of all these parameters at nanosecond time scales (see

[1]Department of Applied Physics, School of Engineering, The University of Tokyo, 7-3-1 Hongo, Bunkyo-ku, Tokyo 113-8656, Japan. [2]Institute of Engineering Innovation, School of Engineering, The University of Tokyo, 2-11-16 Yayoi, Bunkyo-ku, Tokyo 113-8656, Japan. [3]JST, PRESTO, 4-1-8 Honcho, Kawaguchi, Saitama 332-0012, Japan.
*Corresponding author. Email: takeda@ap.t.u-tokyo.ac.jp (S.T.); akiraf@ap.t.u-tokyo.

A

EPR state
GHZ state
Linear-shaped cluster state
Star-shaped cluster state

B

EPR state
3-mode GHZ state
2-mode cluster state
3-mode cluster state
Graph 1
Graph 2
One-dimensional cluster state

Fig. 1. Various types of entanglement. (**A**) Types of entanglement that can be generated by our entanglement synthesizer. (**B**) Types of entanglement that are actually generated and verified in this experiment. Orange spheres represent quantum modes. Blue arrows connecting two modes mean that the connected nodes can communicate with each other by use of the entanglement. Brown links connecting two modes mean that an entangling gate to generate cluster states is applied between these modes.

Materials and Methods). Figure 2E represents the actual response of switching the beam splitter transmissivity in our setup, showing that the switching time is sufficiently short to change the transmissivity from pulse to pulse.

As a demonstration of programmable entanglement generation, we first program the synthesizer to generate five different small-scale entangled states, including an EPR state, a three-mode GHZ state, a two-mode cluster state, and two three-mode cluster states with different graphs, as shown in Fig. 1B (graphs 1 and 2 correspond to the linear and star shape, respectively; see Fig. 1A). To verify generation of the desired entanglement, we apply temporal mode functions to the homodyne signals and extract quadratures $\hat{x}_k$ and $\hat{p}_k$ of the k-th broadband optical pulse, thereby assessing the quadrature correlation between different pulses. The strength of correlation is quantified by inseparability parameters, which are directly linked to the effective level of squeezing and become zero in the limit of infinite squeezing. The inseparability parameter below 1 ($\hbar = 1/2$) is a sufficient condition for the state to be fully inseparable (11, 14, 20, 21). Table 1 summarizes the control sequence of the system parameters as well as the expression and measured values of the inseparability parameter for each state. We see that all the values satisfy the inseparability criteria and demonstrate the programmable generation of five different entangled states. All the values are reasonably well explained by the accumulated loss during the squeezed light generation, entangled state synthesis in the loop, and measurement (see Materials and Methods).

Note that the current experimental setup is unable to synthesize more than three-mode GHZ and cluster states (except for the large-scale cluster state described in the next paragraph) for a technical reason; the switching of $T(t)$ is realized by an electro-optic modulator (EOM), but $T(t)$ is switchable among only three different values because of the design of the EOM driving circuits that we use. By developing a more sophisticated driving circuit or cascading multiple EOMs at the expense of extra loss, we can increase the number of selectable transmissivity values and generate GHZ and cluster states of arbitrary number of modes (see Materials and Methods).

Synthesis of a large-scale cluster state

Our entanglement synthesizer is not limited to producing small-scale entangled states but can produce a large-scale entangled state and thus

has high scalability. We demonstrate this scalability by generating a large-scale one-dimensional cluster state (Fig. 1B), which is known to be a universal resource for single-mode one-way quantum computation for CVs (9). This state can be produced by dynamically controlling the system parameters as $T_1 = 1$, $T_k = (\sqrt{5} - 1)/2$ ($k \geq 2$), and $\theta_k = 90°$ ($k \geq 1$). Under this condition, a one-dimensional cluster state is continuously produced, as shown in Fig. 3A (see Materials and Methods). This circuit is effectively equivalent to the cluster state generation proposed in (22) and demonstrated in (12). The generated state can be characterized by a nullifier $\hat{\delta}_k$, defined as

$$\hat{\delta}_k = \begin{cases} \hat{p}_1 - \hat{x}_2 & (k = 1) \\ \hat{p}_k - \hat{x}_{k-1} - \hat{x}_{k+1} & (k \geq 2) \end{cases} \quad (1)$$

and $\langle \hat{\delta}_k^2 \rangle \to 0$ in the limit of infinite squeezing. The sufficient condition for the state to be inseparable is $\langle \hat{\delta}_k^2 \rangle < 1/2$ for all k (11, 12, 14).

Figure 3B shows the quadratures for the first 15 modes acquired by setting the default measurement basis to $\hat{x}_k$ and switching the basis to $\hat{p}_k$ only when k is even. The quadrature value looks randomly distributed, but once $\hat{x}_{k-1} + \hat{x}_{k+1}$ is calculated and plotted with $\hat{p}_k$ as in Fig. 3C, the correlation between these two values can be observed. This correlation results in the reduction of $\langle \hat{\delta}_k^2 \rangle$ below 1/2 in Fig. 3D, which demonstrates the generation of the one-dimensional cluster state of more than 1000 modes. Because of technical limitations associated with our control sequence, measurement time, and stability of the setup, we stop the measurement at $k = 1008$. In principle, there is no theoretical limitation for the number of entangled modes in this method.

Note that the reduction of $\langle \hat{\delta}_k^2 \rangle$ here (−3.7 dB below the vacuum noise level on average) is slightly weaker than that in (12) (−5 dB at the maximum). Direct comparison of the quality of these cluster states is not possible, but compared to the scheme in (12), our loop-based scheme is more susceptible to losses because additional optical components for the variable beam splitter and phase shifter introduce extra losses and also because the round-trip loss in the loop is accumulated while optical pulses repeatedly circulate there.

## Loop circuit as a quantum memory

The programmable loop circuit further allows us to confine an optical pulse in the loop by keeping $T(t) = 0$ and release it after n loops, effectively acting as a quantum memory. The ability to add a tunable delay to nonclassical CV states plays a key role for time synchronization in various quantum protocols (3, 23, 24), but there have been only a few memory experiments for CV entanglement (25, 26). A loop-based quantum memory is a simple and versatile memory that limits neither the wavelength nor the quantum state of light, but it has been demonstrated only for single photons (27, 28). Here, we demonstrate this functionality by first generating an EPR state in the loop, then storing one part of the EPR state for n loops, and finally releasing it (Fig. 4A). In this scheme, one part of the EPR state is stored, whereas the other is left propagating, which is exactly the same situation as in quantum repeater protocol. We measure the inseparability parameter for the EPR state after introducing the delay $n\tau$. As shown in Fig. 4B, the inseparability parameter is below 1 and satisfies the inseparability criterion up to ~400 ns ($n = 6$), although it gradually degrades as the delay increases. A theoretical simulation shows that the lifetime of the EPR correlation in our system is dominantly limited by the phase fluctuation of ~7° in the loop, rather than the round-trip loss of ~7%.
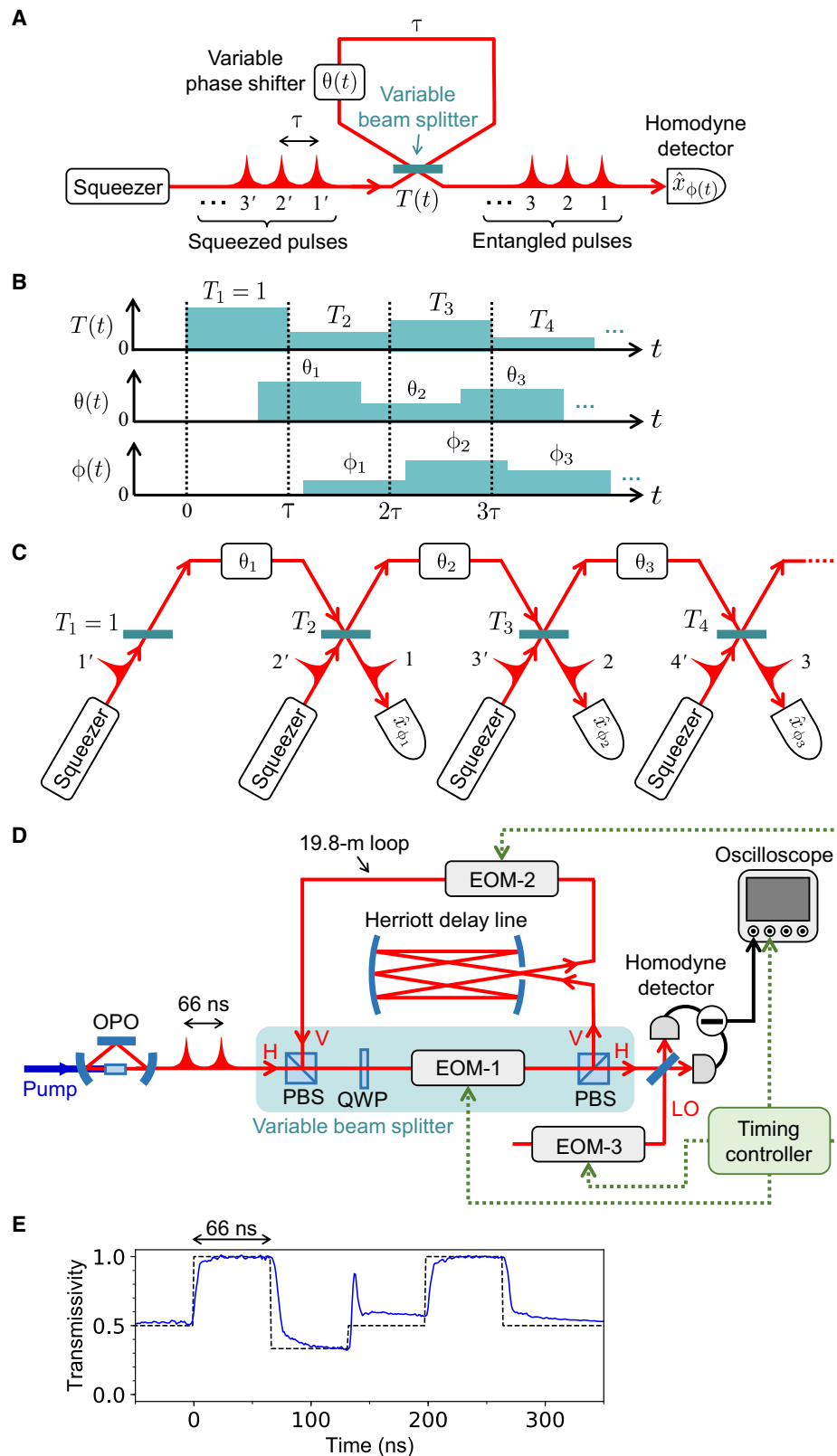
Fig. 2. Schematic of an on-demand entanglement synthesizer. (**A**) Conceptual schematic. (**B**) Time sequence for changing system parameters. (**C**) Equivalent circuit. (**D**) Experimental setup. See Materials and Methods for details. "H" and "V" denote horizontal and vertical polarization, respectively. OPO, optical parametric oscillator; PBS, polarizing beam splitter; QWP, quarter wave plate; EOM, electro-optic modulator; LO, local oscillator. (**E**) Actual control of beam splitter transmissivity $T(t)$. Both measured (blue line) and ideal (black dotted line) responses are plotted.

Table 1. Control sequence and inseparability parameters for various entangled states. $T(t)$ and $\theta(t)$ are controlled by the sequence in Fig. 2B with the setting values $(T_1, T_2, \ldots)$ and $(\theta_1, \theta_2, \ldots)$ defined in this table. $\phi(t)$ is also controlled to measure the inseparability parameter for each state. The generated state is inseparable when each inseparability parameter is below 1 ($h = 1/2$). The expression of inseparability parameters is given in (11, 14, 20, 21).

| Type of entanglement	$(T_1, T_2, \ldots)$	$(\theta_1, \theta_2, \ldots)$	Inseparability parameter	Measured value
EPR state	$(1, \frac{1}{2}, 1)$	$(90°, 0°)$	$\langle[\Delta(\hat{x}_1 - \hat{x}_2)]^2\rangle + \langle[\Delta(\hat{p}_1 + \hat{p}_2)]^2\rangle$	0.44 ± 0.01
3-mode GHZ state	$(1, \frac{1}{3}, \frac{1}{2}, 1)$	$(90°, 180°, 0°)$	$\langle[\Delta(\hat{x}_1 - \hat{x}_2)]^2\rangle + \langle[\Delta(\hat{p}_1 + \hat{p}_2 + \hat{p}_3)]^2\rangle$	0.65 ± 0.01
			$\langle[\Delta(\hat{x}_2 - \hat{x}_3)]^2\rangle + \langle[\Delta(\hat{p}_1 + \hat{p}_2 + \hat{p}_3)]^2\rangle$	0.67 ± 0.01
			$\langle[\Delta(\hat{x}_1 - \hat{x}_3)]^2\rangle + \langle[\Delta(\hat{p}_1 + \hat{p}_2 + \hat{p}_3)]^2\rangle$	0.70 ± 0.01
2-mode cluster state	$(1, \frac{1}{2}, 1)$	$(90°, 90°)$	$\langle[\Delta(\hat{p}_1 - \hat{x}_2)]^2\rangle + \langle[\Delta(\hat{p}_2 - \hat{x}_1)]^2\rangle$	0.42 ± 0.01
3-mode cluster state (graph 1)	$(1, \frac{2}{3}, \frac{1}{2}, 1)$	$(90°, 90°, 90°)$	$\langle[\Delta(\hat{p}_1 - \hat{x}_2)]^2\rangle + \langle[\Delta(\hat{p}_2 - \hat{x}_1 - \hat{x}_3)]^2\rangle$	0.56 ± 0.01
			$\langle[\Delta(\hat{p}_3 - \hat{x}_2)]^2\rangle + \langle[\Delta(\hat{p}_2 - \hat{x}_1 - \hat{x}_3)]^2\rangle$	0.54 ± 0.01
			$\langle[\Delta(\hat{p}_1 - \hat{p}_3)]^2\rangle + \langle[\Delta(\hat{p}_2 - \hat{x}_1 - \hat{x}_3)]^2\rangle$	0.60 ± 0.01
3-mode cluster state (graph 2)	$(1, \frac{1}{3}, \frac{1}{2}, 1)$	$(90°, 180°, 90°)$	$\langle[\Delta(\hat{p}_1 - \hat{x}_3)]^2\rangle + \langle[\Delta(\hat{p}_3 - \hat{x}_1 - \hat{x}_2)]^2\rangle$	0.69 ± 0.01
			$\langle[\Delta(\hat{p}_2 - \hat{x}_3)]^2\rangle + \langle[\Delta(\hat{p}_3 - \hat{x}_1 - \hat{x}_2)]^2\rangle$	0.65 ± 0.01
			$\langle[\Delta(\hat{p}_1 - \hat{p}_2)]^2\rangle + \langle[\Delta(\hat{p}_3 - \hat{x}_1 - \hat{x}_2)]^2\rangle$	0.63 ± 0.01
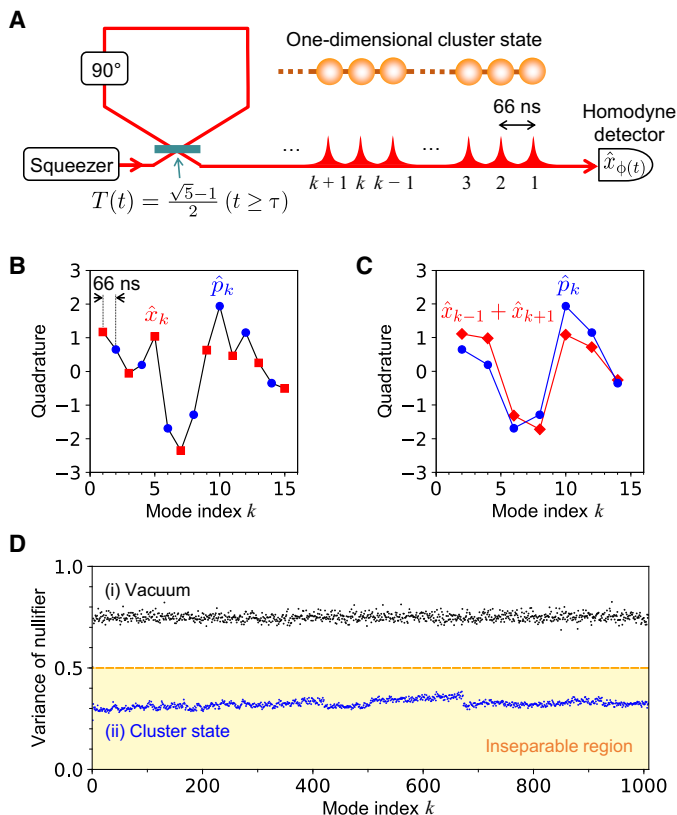
Fig. 3. Generation of a one-dimensional cluster state. (A) Schematic. **(B)** Single-shot measurement of quadratures for the first 15 modes. $\hat{x}_k$ ($\hat{p}_k$) is measured for odd (even) number modes and plotted as red squares (blue circles). **(C)** Comparison between $\hat{p}_k$ (blue circles) and $\hat{x}_{k-1} + \hat{x}_{k+1}$ (red diamonds). **(D)** Measured variance of nullifier $\langle \hat{\delta}_k^2 \rangle$ for (i) vacuum states (as a reference; black dots) and (ii) cluster states (blue dots). The SE of each variance is around 0.01 and always below 0.03. The yellow shaded area represents the inseparable region.

Specifically, a small phase drift in the loop is accumulated when the stored pulse circulates in the loop, destroying the relative phase relation between two EPR pulses. As a result, the measured inseparability parameter is contaminated by the noise of anti-squeezed quadratures and finally exceeds 1 after ~400 ns. Therefore, the lifetime of our memory can be increased by improving the mechanical stability of the loop or the feedback system to stabilize the phase. Our loop-based memory can store any CV quantum states, such as non-Gaussian states, by changing our squeezer to other quantum light sources (29).

DISCUSSION

In conclusion, we have programmably generated and verified a variety of small- and large-scale entangled states by dynamically controlling the beam splitter transmissivity, phase shift, and measurement basis of a loop-based optical circuit at nanosecond time scales. We have also demonstrated that this circuit can work as a quantum memory by storing one part of an EPR state in the loop. Our loop-based system is programmable and highly scalable, offering a unique and versatile tool for future photonic quantum technologies.

The demonstrated circuit is a core circuit to build more general photonic circuits. By embedding this loop circuit in another large loop, we can realize an arbitrary beam splitter network to combine input squeezed pulses (17), thereby synthesizing more general entangled states including an arbitrary cluster state (8). Moreover, this circuit can be further extended to a universal quantum computer by incorporating a programmable displacement operation based on the homodyne detector's signal and another non-Gaussian light source (18). In these schemes, fault-tolerant quantum computation is possible even with finite level of squeezing (18, 30). Our demonstration is a crucial step to realize these goals and will stimulate further theoretical and experimental research toward scalable photonic quantum information processing.
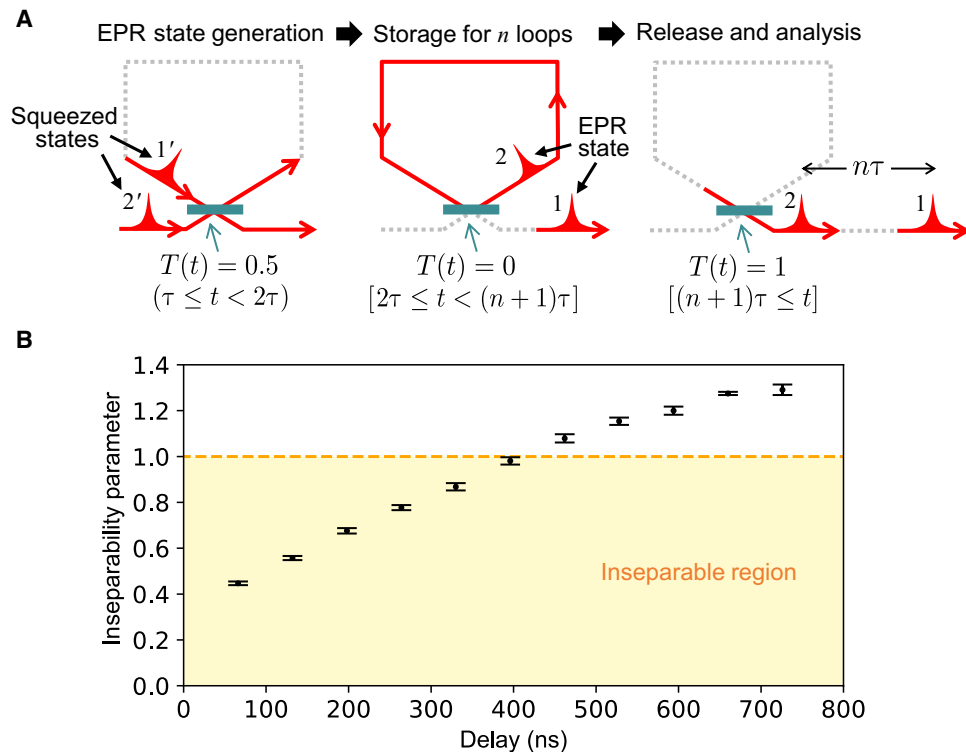
Fig. 4. Storage of one part of an EPR state in the loop. (A) Control sequence. **(B)** Measured inseparability parameter $\langle[\Delta(\hat{x}_1 - \hat{x}_2)]^2\rangle + \langle[\Delta(\hat{p}_1 + \hat{p}_2)]^2\rangle$ with SE is plotted for each delay $n\tau$ ($\tau = 66$ ns, $n = 1, 2, \ldots, 11$). The yellow shaded area represents the inseparable region.

MATERIALS AND METHODS

Experimental setup and data analysis

We used a continuous-wave Ti:sapphire laser at 860 nm. Our optical parametric oscillator [OPO; the same design as in (31)] produced a squeezed light with ~5 dB of squeezing and ~8 dB of anti-squeezing at low frequencies (this means ~9 dB of pure squeezing and the total loss of ~20% during the generation and measurement process). Our loop, built by a Herriott-type optical delay line (32), has a round-trip length of 19.8 m and a round-trip loss of ~7% . Considering this loop length, we artificially divided the squeezed light into 66-ns time bins. Each time bin was further divided into 20-ns switching time used for changing system parameters and 46-ns processing time within which a squeezed optical pulse was defined. The loop includes a variable beam splitter composed of two polarizing beam splitters (PBSs) and one bulk-type polarization-rotation EOM. By inserting a quarter wave plate (QWP) between the PBSs, the transmissivity of the beam splitter was initially set to 0.5, and the EOM changed the transmissivity when it was triggered. The variable phase shifter was realized by a bulk-type phase-modulation EOM, shifting the phase from the initially locked value of 0° when it was triggered. Last, the pulses after the loop were mixed with a local oscillator (LO) beam and measured using a homodyne detector. Here, a waveguide-type EOM in the LO's path can shift the phase $\phi(t)$ and thereby change the measurement basis $\hat{x}_{\phi(t)}$. During the measurement, we periodically switched between two different settings at a rate of 2 kHz; one is the feedback setting when the cavity length of the OPO and the relative phases of beams were actively locked by weakly injected reference beams, and the other is the measurement setting when the control sequence in Fig. 2B was triggered and the data were acquired without the reference beams (12).

To analyze the generated states, we acquired the homodyne detector's signal using an oscilloscope at a sampling rate of 1.25 GHz. Five thousand data frames were recorded to estimate each inseparability parameter and nullifier. The quadrature of the k-th mode was extracted by applying a temporal mode function $f_k(t)$ to each data frame, defined as (33)

$$f_k(t) \propto \begin{cases} e^{-\gamma^2(t-t_k)^2}(t - t_k) & (2\,|\,t - t_k\,| \leq T) \\ 0 & (\text{otherwise}) \end{cases} \quad (2)$$

and normalized to be $\int_{-\infty}^{\infty} |f_k(t)|^2 dt = 1$. The parameters used in this experiment are $T = 46$ ns, $\gamma = 6 \times 10^7$ /s, and $t_k = t_0 + (k - 1)\tau$, where t_0 is the optimized center position of the first mode and $\tau = 66$ ns is the interval between the modes. Using these parameters, we checked the orthogonality of the neighboring modes by applying $f_k(t)$ to the data frames for the shot noise signal and confirming that the quadrature correlation between different modes is negligible (33).

Working principle of variable beam splitter and phase shifter

The EOMs for the variable beam splitter and phase shifter contain a crystal of rubidium titanyl phosphate that is sandwiched between two electrodes. We used commercially available EOM driving circuits that are composed of two fast high-voltage switches (one for each electrode). These switches enabled us to selectively apply 0 or V_1 volt to one of these electrodes and 0 or $-V_2$ volt to the other electrode, where $V_1 > 0$ and $V_2 > 0$ can be arbitrarily chosen in advance. The net voltage applied to the crystal can thus be switched among 0, V_1,

V_2, and $V_1 + V_2$, and these voltages determine the possible values of $T(t)$ and $\theta(t)$. The rise/fall time for the switching is ~10 ns. In this system, it is not possible to switch $T(t)$ and $\theta(t)$ among more than three different target values in general because of the design of the EOM driving circuits. As a result, our setup was unable to generate GHZ or cluster states of more than three modes, which require switching of $T(t)$ among four or more different values. This limitation can be overcome by developing another sophisticated EOM driving circuits containing more high-voltage switches to increase the number of selectable voltages. Another solution is to cascade multiple EOMs at the expense of introducing additional transmission loss. Because one EOM can shift $T(t)$ from the initial value (applied voltage, 0 volt) to two different target values (V_1 or V_2 volt), n cascaded EOMs make it possible to switch $T(t)$ among $2n + 1$ different target values. In this way, GHZ or cluster states of arbitrary number of modes can be generated in principle.

In the following, we introduce theoretical description of the action of the variable beam splitter and phase shifter. In Fig. 2C, the k-th beam splitter with transmissivity T_k ($k \geq 2$) mixes one mode from a squeezer (annihilation operator $\hat{a}'_k = \hat{x}'_k + i\hat{p}'_k$) and the other mode coming from the ($k - 1$)-th beam splitter ($\hat{a}''_{k-1}$). After this operation, one of the output modes is measured ($\hat{a}_{k-1} = \hat{x}_{k-1} + i\hat{p}_{k-1}$), while the other output mode become the input mode of the ($k + 1$)-th beam splitter after the phase shift of θ_k ($\hat{a}''_k$). In Fig. 2D, the same operation is performed with the variable beam splitter and variable phase shifter. In the variable beam splitter, the QWP initially introduces a relative phase offset of 90° between two diagonal polarizations, thereby setting the default transmissivity to 0.5. The polarization-rotation EOM introduces an additional relative phase shift of $2\delta_k \geq 0$, which is proportional to the applied voltage. Under this condition, the function of the k-th beam splitter and phase shifter in Fig. 2C is realized in Fig. 2D as

$$\begin{pmatrix} \hat{a}_{k-1} \\ \hat{a}''_k \end{pmatrix} = \begin{pmatrix} 1 & 0 \\ 0 & e^{i\theta_k} \end{pmatrix} \begin{pmatrix} \sin(\delta_k + 45°) & -\cos(\delta_k + 45°) \\ \cos(\delta_k + 45°) & \sin(\delta_k + 45°) \end{pmatrix} \begin{pmatrix} \hat{a}''_{k-1} \\ \hat{a}'_k \end{pmatrix} \tag{3}$$

The transmissivity of the variable beam splitter is defined by $T_k = \sin^2(\delta_k + 45°)$ in Eq. 3. By gradually increasing the applied voltage and thereby increasing δ_k from 0° to 45°, T_k can be increased from 0.5 to 1. Thus, any transmissivity between 0.5 and 1 can be chosen in this way. When the transmissivity between 0 and 0.5 is required, the voltage has to be further increased to set δ_k between 90° and 135°. In this region, however, the sign of the off-diagonal terms in Eq. 3 flips. This sign flip corresponds to the additional phase shift of 180˚ before and after the beam splitter operation

$$\begin{pmatrix} \sqrt{T_k} & \sqrt{1 - T_k} \\ -\sqrt{1 - T_k} & \sqrt{T_k} \end{pmatrix} = \begin{pmatrix} 1 & 0 \\ 0 & -1 \end{pmatrix} \begin{pmatrix} \sqrt{T_k} & -\sqrt{1 - T_k} \\ \sqrt{1 - T_k} & \sqrt{T_k} \end{pmatrix} \begin{pmatrix} 1 & 0 \\ 0 & -1 \end{pmatrix} \tag{4}$$

Generation of GHZ and star-shaped cluster states

It is known that an n-mode GHZ state ($n \geq 2$; the case of $n = 2$ corresponds to an EPR state) can be generated in the setup of Fig. 2C by setting $T_1 = T_{n+1} = 1$, $T_k = 1/(n - k + 2)$ ($2 \leq k \leq n$), and $\theta_1 = 90°$, $\theta_k = 0$ ($2 \leq k \leq n$) (5). When all input modes are infinitely $\hat{x}$-squeezed vac-

uum states (the input quadratures satisfy $\hat{x}'_k = 0$ for all k), the quadratures of the output modes in this setting show the correlation of the GHZ state

$$\hat{x}_k - \hat{x}_n = 0 \ (1 \leq k \leq n - 1), \sum_{k=1}^{n} \hat{p}_k = 0 \tag{5}$$

Here, we show that the difference between the n-mode GHZ state and the n-mode star-shaped cluster state is only local phase shifts. We replace $\hat{x}_l \rightarrow \hat{p}_l$ and $\hat{p}_l \rightarrow -\hat{x}_l$ for all l in Eq. 5 by redefining the quadratures. We then introduce an additional phase rotation of $\theta_n = 90°$ to undo this replacement only for the n-th mode. After these operations, Eq. 5 transforms into

$$\hat{p}_k - \hat{x}_n = 0 \ (1 \leq k \leq n - 1), \hat{p}_n - \sum_{k=1}^{n-1} \hat{x}_k = 0 \tag{6}$$

which are the definition of the n-mode star-shaped cluster state in Fig. 1A. Therefore, the actual difference of the settings for generating GHZ and star-shaped cluster states is only the value of θ_n.

In this experiment, these settings were used for generating the EPR state, three-mode GHZ state, two-mode cluster state, and three-mode cluster state (graph 2). When we generated three-mode GHZ and cluster states (graph 2), additional phase shifts of 180° before and after the beam splitter were introduced by the variable beam splitter with $T_2 = 1/3$, as explained in Eq. 4. The 180° phase shift before the beam splitter had no effect because it was applied to a squeezed vacuum state with 180° rotational symmetry, and the phase shift after the beam splitter was cancelled out by setting $\theta_2 = 180°$, as shown in Table 1.

Generation of linear-shaped cluster states

The setup of Fig. 2C can also produce an n-mode linear-shaped cluster state by setting $T_1 = T_{n+1} = 1$, $T_k = F_{n-k+2}/F_{n-k+3}$ ($2 \leq k \leq n$), and $\theta_k = 90°$ ($1 \leq k \leq n$) (19). Here, F_k is a Fibonacci number defined by $F_0 = 0$, $F_1 = 1$, $F_k = F_{k-1} + F_{k-2}$ ($k \geq 2$) and given by

$$F_k = \frac{1}{\sqrt{5}}\left[\left(\frac{1 + \sqrt{5}}{2}\right)^k - \left(\frac{1 - \sqrt{5}}{2}\right)^k \right] \tag{7}$$

In this setting, the k-th beam splitter with $T_k = F_{n-k+2}/F_{n-k+3}$, followed by the k-th phase shifter with $\theta_k = 90°$, transforms the annihilation operators as

$$\begin{aligned} \begin{pmatrix} \hat{a}_{k-1} \\ \hat{a}''_k \end{pmatrix} &= \begin{pmatrix} 1 & 0 \\ 0 & i \end{pmatrix} \begin{pmatrix} \sqrt{T_k} & -\sqrt{1 - T_k} \\ \sqrt{1 - T_k} & \sqrt{T_k} \end{pmatrix} \begin{pmatrix} \hat{a}''_{k-1} \\ \hat{a}'_k \end{pmatrix} \\ &= \frac{1}{\sqrt{F_{n-k+3}}} \begin{pmatrix} \sqrt{F_{n-k+2}} & -\sqrt{F_{n-k+1}} \\ i\sqrt{F_{n-k+1}} & i\sqrt{F_{n-k+2}} \end{pmatrix} \begin{pmatrix} \hat{a}''_{k-1} \\ \hat{a}'_k \end{pmatrix} \end{aligned} \tag{8}$$

In the setup of Fig. 2C, this transformation is cascaded from $k = 2$ to $k = n$ after the phase rotation $\theta_1 = 90°$ of the first mode ($\hat{a}''_1 = i\hat{a}'_1$). After these transformations, the output annihilation operator of the k-th mode is given by

$$\hat{a}_k = \frac{i^k F_{n-k+1}}{\sqrt{F_n F_{n+1}}}\hat{a}'_1 + \sum_{l=2}^{k} \frac{i^{k-l+1} F_{n-k+1}}{\sqrt{F_{n-l+1} F_{n-l+3}}}\hat{a}'_l - \sqrt{\frac{F_{n-k}}{F_{n-k+2}}}\hat{a}'_{k+1} \tag{9}$$

When all input modes are infinitely $\hat{x}$-squeezed vacuum states ($\hat{x}'_k = 0$ for all k), it can be proven from Eq. 9 that the quadratures of the output modes satisfy

$$\hat{p}_1 - \hat{x}_2 = 0, \hat{p}_n - \hat{x}_{n-1} = 0$$

$$\hat{p}_k - \hat{x}_{k-1} - \hat{x}_{k+1} = 0 \ (2 \leq k \leq n-1) \quad (10)$$

which are the definition of the n-mode linear cluster state in Fig. 1A. This setting was used for generating the three-mode cluster state (graph 1) in this experiment.

In this method, the transmissivity T_k approaches a constant value $(\sqrt{5} - 1)/2$ in the limit of $n \to \infty$. This means that the linear cluster state is unlimitedly generated by fixing $T_k = (\sqrt{5} - 1)/2$ for all $k \geq 2$, satisfying

$$\hat{p}_1 - \hat{x}_2 = 0, \hat{p}_k - \hat{x}_{k-1} - \hat{x}_{k+1} = 0 \ (k \geq 2) \quad (11)$$

This method was used for generating a one-dimensional cluster state in Fig. 3A.

REFERENCES AND NOTES

1. A. Einstein, B. Podolsky, N. Rosen, Can quantum-mechanical description of physical reality be considered complete? *Phys. Rev.* **47**, 777–780 (1935).
2. A. Furusawa, J. L. Sørensen, S. L. Braunstein, C. A. Fuchs, H. J. Kimble, E. S. Polzik, Unconditional quantum teleportation. *Science* **282**, 706–709 (1998).
3. S. D. Bartlett, W. J. Munro, Quantum teleportation of optical quantum gates. *Phys. Rev. Lett.* **90**, 117901 (2003).
4. D. M. Greenberger, M. A. Horne, A. Shimony, A. Zeilinger, Bell's theorem without inequalities. *Am. J. Phys.* **58**, 1131–1143 (1990).
5. P. van Loock, S. L. Braunstein, Multipartite entanglement for continuous variables: A quantum teleportation network. *Phys. Rev. Lett.* **84**, 3482–3485 (2000).
6. M. Hillery, V. Bužek, A. Berthiaume, Quantum secret sharing. *Phys. Rev. A* **59**, 1829–1834 (1999).
7. R. Raussendorf, H. J. Briegel, A one-way quantum computer. *Phys. Rev. Lett.* **86**, 5188–5191 (2001).
8. P. van Loock, C. Weedbrook, M. Gu, Building Gaussian cluster states by linear optics. *Phys. Rev. A* **76**, 032321 (2007).
9. N. C. Menicucci, P. van Loock, M. Gu, C. Weedbrook, T. C. Ralph, M. A. Nielsen, Universal quantum computation with continuous-variable cluster states. *Phys. Rev. Lett.* **97**, 110501 (2006).
10. T. Aoki, N. Takei, H. Yonezawa, K. Wakui, T. Hiraoka, A. Furusawa, P. van Loock, Experimental creation of a fully inseparable tripartite continuous-variable state. *Phys. Rev. Lett.* **91**, 080404 (2003).
11. M. Yukawa, R. Ukai, P. van Loock, A. Furusawa, Experimental generation of four-mode continuous-variable cluster states. *Phys. Rev. A* **78**, 012301 (2008).
12. S. Yokoyama, R. Ukai, S. C. Armstrong, C. Sornphiphatphong, T. Kaji, S. Suzuki, J. Yoshikawa, H. Yonezawa, N. C. Menicucci, A. Furusawa, Ultra-large-scale continuous-variable cluster states multiplexed in the time domain. *Nat. Photonics* **7**, 982–986 (2013).
13. M. Chen, N. C. Menicucci, O. Pfister, Experimental realization of multipartite entanglement of 60 modes of a quantum optical frequency comb. *Phys. Rev. Lett.* **112**, 120505 (2014).
14. S. Armstrong, J.-F. Morizur, J. Janousek, B. Hage, N. Treps, P. K. Lam, H.-A. Bachor, Programmable multimode quantum networks. *Nat. Commun.* **3**, 1026 (2012).
15. J. Roslund, R. M. de Araújo, S. Jiang, C. Fabre, N. Treps, Wavelength-multiplexed quantum networks with ultrafast frequency combs. *Nat. Photonics* **8**, 109–112 (2014).
16. Y. Cai, J. Roslund, G. Ferrini, F. Arzani, X. Xu, C. Fabre, N. Treps, Multimode entanglement in reconfigurable graph states using optical frequency combs. *Nat. Commun.* **8**, 15645 (2017).
17. K. R. Motes, A. Gilchrist, J. P. Dowling, P. Rohde, Scalable boson sampling with time-bin encoding using a loop-based architecture. *Phys. Rev. Lett.* **113**, 120501 (2014).
18. S. Takeda, A. Furusawa, Universal quantum computing with measurement-induced continuous-variable gate sequence in a loop-based architecture. *Phys. Rev. Lett.* **119**, 120504 (2017).
19. R. Ukai, *Multi-Step Multi-Input One-Way Quantum Information Processing with Spatial and Temporal Modes of Light* (Springer, 2015).
20. L.-M. Duan, G. Giedke, J. I. Cirac, P. Zoller, Inseparability criterion for continuous variable systems. *Phys. Rev. Lett.* **84**, 2722–2725 (2000).
21. P. van Loock, A. Furusawa, Detecting genuine multipartite continuous-variable entanglement. *Phys. Rev. A* **67**, 052315 (2003).
22. N. C. Menicucci, X. Ma, T. C. Ralph, Arbitrarily large continuous-variable cluster states from a single quantum nondemolition gate. *Phys. Rev. Lett.* **104**, 250503 (2010).
23. D. Gottesman, A. Kitaev, J. Preskill, Encoding a qubit in an oscillator. *Phys. Rev. A* **64**, 012310 (2001).
24. J. B. Brask, I. Rigas, E. S. Polzik, U. L. Andersen, A. S. Sørensen, Hybrid long-distance entanglement distribution protocol. *Phys. Rev. Lett.* **105**, 160501 (2010).
25. A. M. Marino, R. C. Pooser, V. Boyer, P. D. Lett, Tunable delay of Einstein-Podolsky-Rosen entanglement. *Nature* **457**, 859–862 (2009).
26. K. Jensen, W. Wasilewski, H. Krauter, T. Fernholz, B. M. Nielsen, M. Owari, M. B. Plenio, A. Serafini, M. M. Wolf, E. S. Polzik, Quantum memory for entangled continuous-variable states. *Nat. Phys.* **7**, 13–16 (2011).
27. T. B. Pittman, B. C. Jacobs, J. D. Franson, Single photons on pseudodemand from stored parametric down-conversion. *Phys. Rev. A* **66**, 042303 (2002).
28. F. Kaneda, B. G. Christensen, J. J. Wong, H. S. Park, K. T. McCusker, P. G. Kwiat, Time-multiplexed heralded single-photon source. *Optica* **2**, 1010–1013 (2015).
29. M. Yukawa, K. Miyata, T. Mizuta, H. Yonezawa, P. Marek, R. Filip, A. Furusawa, Generating superposition of up-to three photons for continuous variable quantum information processing. *Opt. Express* **21**, 5529–5535 (2013).
30. N. C. Menicucci, Fault-tolerant measurement-based quantum computing with continuous-variable cluster states. *Phys. Rev. Lett.* **112**, 120504 (2014).
31. Y. Shiozawa, J. Yoshikawa, S. Yokoyama, T. Kaji, K. Makino, T. Serikawa, R. Nakamura, S. Suzuki, S. Yamazaki, W. Asavanant, S. Takeda, P. van Loock, A. Furusawa, Quantum nondemolition gate operations and measurements in real time on fluctuating signals. *Phys. Rev. A* **98**, 052311 (2018).
32. D. Herriott, H. Kogelnik, R. Kompfner, Off-axis paths in spherical mirror interferometers. *Appl. Optics* **3**, 523–526 (1964).
33. J. Yoshikawa, S. Yokoyama, T. Kaji, C. Sornphiphatphong, Y. Shiozawa, K. Makino, A. Furusawa, Invited article: Generation of one-million-mode continuous-variable cluster state by unlimited time-domain multiplexing. *APL Photonics* **1**, 060801 (2016).

Science Advances

On-demand photonic entanglement synthesizer

Shuntaro Takeda, Kan Takase and Akira Furusawa

ARTICLE TOOLS	http://advances.sciencemag.org/content/5/5/eaaw4530
REFERENCES	This article cites 32 articles, 1 of which you can access for free http://advances.sciencemag.org/content/5/5/eaaw4530#BIBL
PERMISSIONS	http://www.sciencemag.org/help/reprints-and-permissions